Article:
Gregory, T Stan, Murrow, Jonathan R, Oshinski, John N et al. (1 more author) (2019) Exploring magnetohydrodynamic voltage distributions in the human body:Preliminary results. PLoS ONE. e0213235. ISSN 1932-6203

https://doi.org/10.1371/journal.pone.0213235

PLOS ONE

RESEARCH ARTICLE

Exploring magnetohydrodynamic voltage distributions in the human body: Preliminary results

T. Stan Gregory[1], Jonathan R. Murrow[2], John N. Oshinski[3], Zion Tsz Ho Tse[4]*

1 College of Engineering, University of Georgia, Athens, Georgia, United States of America, **2** AU/UGA Medical Partnership, University of Georgia, Athens, Georgia, United States of America, **3** Department of Radiology and Imaging Sciences, Emory University, Atlanta, Georgia, United States of America, **4** School of Electrical and Computer Engineering, University of Georgia, Athens, Georgia, United States of America

* ziontse@uga.edu

Citation: Gregory TS, Murrow JR, Oshinski JN, Tse ZTH (2019) Exploring magnetohydrodynamic voltage distributions in the human body: Preliminary results. PLoS ONE 14(3): e0213235. https://doi.org/10.1371/journal.pone.0213235

Editor: Lucio Careddu, Policlinico S. Orsola-Malpighi, ITALY

Received: June 16, 2017

Accepted: February 19, 2019

Published: March 6, 2019

Data Availability Statement: All relevant data are within the paper.

Funding: This study was supported in part by the National Institutes of Health (NIH) Bench-to-Bedside Award, the NIH Center for Interventional Oncology Grant, the National Science Foundation (NSF) I-Corps Team Grant (1617340), NSF REU site program 1359095, the UGA-AU Inter-Institutional Seed Funding, the American Society for Quality Dr. Richard J. Schlesinger Grant, the PHS Grant UL1TR000454 from the Clinical and Translational Science Award Program of the NIH

Abstract

Background

The aim of this study was to noninvasively measure regional contributions of vasculature in the human body using magnetohydrodynamic voltages (V_{MHD}) obtained from electrocardiogram (ECG) recordings performed inside MRI's static magnetic field (B_0). Integrating the regional V_{MHD} over the S_{wave}-T_{wave} segment of the cardiac cycle ($V_{segment}$) provides a non-invasive method for measuring regional blood volumes, which can be rapidly obtained during MRI without incurring additional cost.

Methods

V_{MHD} was extracted from 12-lead ECG traces acquired during gradual introduction into a 3T MRI. Regional contributions were computed utilizing weights based on B_0's strength at specified distances from isocenter. $V_{segment}$ mapping was performed in six subjects and validated against MR angiograms (MRA).

Results

Fluctuations in $V_{segment}$, which presented as positive trace deflections, were found to be associated with aortic-arch flow in the thoracic cavity, the main branches of the abdominal aorta, and the bifurcation of the common iliac artery. The largest fluctuation corresponded to the location where the aortic arch was approximately orthogonal to B_0. The smallest fluctuations corresponded to areas of vasculature that were parallel to B_0. Significant correlations (specifically, Spearman's ranked correlation coefficients of 0.96 and 0.97 for abdominal and thoracic cavities, respectively) were found between the MRA and $V_{segment}$ maps ($p < 0.001$).

Conclusions

A novel non-invasive method to extract regional blood volumes from ECGs was developed and shown to be a rapid means to quantify peripheral and abdominal blood volumes.

National Center for Advancing Translational Sciences. The funders had no role in study design, data collection and analysis, decision to publish, or preparation of the manuscript.

Competing interests: The authors have declared that no competing interests exist.

Introduction

This study aims to develop a noninvasive, MRI-compatible method for measuring regional blood volumes. Such a technology could be used to monitor risk factors for and track the progression of cardiovascular disease [1–6]. In addition, longitudinal usage might enable monitoring of wound healing [7]. This technique could be used during patient insertion into the MRI bore prior to the start of a new MRI study, providing additional information without any additional cost. In the future, the technique might also be applied using a static (neodymium) magnetic field source and a stand-alone hand-held device containing miniaturized ECG hardware, which would reduce the cost associated with utilizing an MRI scanner [8].

Our approach is inspired by past studies on utilizing electromagnetics to measure blood flow [9, 10]. The proposed technology is based on the magnetohydrodynamic (MHD) effect, a phenomenon in which the flow of charged particles in a direction perpendicular to a magnetic field creates an electric field in a direction which is mutually perpendicular to both the magnetic field and the flow [11]. A magnetic resonance imaging (MRI) scanner has a very strong static magnetic field ($\vec{B_0}$), which at the center of the magnet is uniform and oriented along the shaft of the MRI bore, while at both ends of the bore it wraps around the exterior of the magnet, rapidly changing in strength and orientation. Induced MHD voltages (V_{MHD}) are directly related to fluid velocity ($\vec{u}$), magnetic flux density ($\vec{B_0}$), and measurement electrode spacing (L) (Eq 1) [12–15].

$$V_{MHD} = \int_0^L (\vec{u} \times \vec{B_0}) \cdot \vec{dL} \quad (1)$$

A well-known example of V_{MHD} arises when the human heart is placed at the center of the MRI scanner, where rapid ejection of blood from the left ventricle into the aortic arch induces a large V_{MHD}, primarily because a sizeable length (5–10 cm) of the wide (~2 cm diameter) arch lies perpendicular to the magnetic field and the flow velocity is high (>100 cm/s). This V_{MHD} appears as a voltage overlaid on top of conventional electrocardiogram (ECG) traces measured inside the MRI bore, which peaks during cardiac systole [11, 12, 16–18]. Using a flow phantom placed inside an MRI, as well as a pump which provided pulsatile flow, V_{MHD} was reproduced in vitro. In addition, the correlation between V_{MHD} observed on conventional ECG traces and cardiac blood flow was demonstrated [19]. Current modeling approaches have been able to successfully simulate the induced V_{MHD} as a linear combination of the true ECG signal and a V_{MHD} term (Eq 1) with an additional scaling factor which was dependent on the measurement electrode selected [20]. Induced V_{MHD} was shown to increase with cross-sectional area and vessel diameter [20, 21]. As predicted, induced V_{MHD} increases as the MRI field strength increases [22, 23].

We hypothesized that monitoring the induced V_{MHD} during the incremental introduction of the human body into the MRI bore from regions completely outside the magnetic field afford an opportunity to assess regional vasculature contributions to the MHD effect, and to further utilize this data in order to assess blood volumes in various portions of the vasculature. A novel non-invasive method to extract regional blood volumes from ECGs was successfully developed and shown to be a rapid means to quantify peripheral and abdominal blood volumes.

Methods

The study was conducted using a Signa HDx 3T MRI scanner (General Electric Healthcare, Waukesha, WI). A 12-lead ECG recording system, modified to be MR Conditional [24], was used to record the 12-lead ECGs of 6 volunteer subjects at 3T (Table 1).

Table 1. Body type and size of each volunteer subject.

	Gender	Age	Height (cm)	Weight (kg)
Subject #1	F	38	159	54.5
Subject #2	M	30	168	68.0
Subject #3	M	25	160	75.8
Subject #4	M	23	179	62.6
Subject #5	M	26	182	77.1
Subject #6	M	22	175	65.2

https://doi.org/10.1371/journal.pone.0213235.t001

The human clinical trials in this study were approved by the University of Georgia Office of Research Institutional Review Board (IRB), and registered with the IRB (registration number: STUDY00003158) on 4/13/2016. Informed consent to participate in the study was obtained from all participants (or their parent or legal guardian in the case of children under 16). The consent forms are held by the authors and are available for review by the Editor-in-Chief. Written informed consent was obtained from all study volunteers for publication of their individual details and accompanying images in this manuscript (as per IRB procedures). The consent forms are held by the authors and are available for review by the Editor-in-Chief.

12-lead ECG patient monitoring was used as it is a clinical standard for cardiac monitoring that measures high-fidelity multi-channel bioelectric potentials at different physiological landmark positions of the thorax. As the study focused on the development of a new methodology for blood volume monitoring with a limited number of volunteer subjects, normal subjects without any prior history of cardiovascular diseases were chosen.

Extraction of MHD voltage distributions

Baseline ECG recordings were obtained for each patient with the patient in the supine position outside the 5-gauss line of the MRI magnetic field. Subjects were placed supine on the MRI scanner table, in a feet-first orientation, with the table in a locked position and the cradle maximally extended out of the bore. The cradle was then advanced into the MRI, progressively bringing more parts of the human body into the MRI scanner's fringe magnetic field, such that the induced V_{MHD} was observed to grow to beyond 5% of the ECG QRS complex. Introduction into the scanner bore was performed in 10-cm increments in five subjects (n = 5), terminating when the heart reached the scanner iso-center (Fig 1a). A higher-spatial-resolution dataset was recorded for an additional subject (n = 1) at 1-cm increments.

12-lead ECG recordings during 20-second breath holds were obtained at each position, characterized by its displacement from the MRI bore isocenter (displacement level). As this study focused on effects of the MRI magnetic field on 12-lead ECG recordings, data was obtained in the absence of MRI gradient pulses (i.e. without the occurrence of imaging). Twelve-lead ECG traces were converted into the VCG domain using an inverse Dower transform, providing a 3-component vector signal representation, $[VCG_X(t)\ VCG_Y(t)\ VCG_Z(t)]$ [25].

$$\begin{bmatrix} VCG_X \\ VCG_Y \\ VCG_Z \end{bmatrix} = \begin{bmatrix} -0.172 & -0.074 & 0.122 & 0.231 & 0.239 & 0.194 & 0.156 & -0.010 \\ 0.057 & -0.019 & -0.106 & -0.022 & 0.041 & 0.048 & -0.227 & 0.887 \\ -0.229 & -0.310 & -0.246 & -0.063 & 0.055 & 0.108 & 0.022 & 0.102 \end{bmatrix} \begin{bmatrix} ECG_I \\ ECG_{II} \\ ECG_{V1} \\ ECG_{V2} \\ ECG_{V3} \\ ECG_{V4} \\ ECG_{V5} \\ ECG_{V6} \end{bmatrix} \quad (2)$$

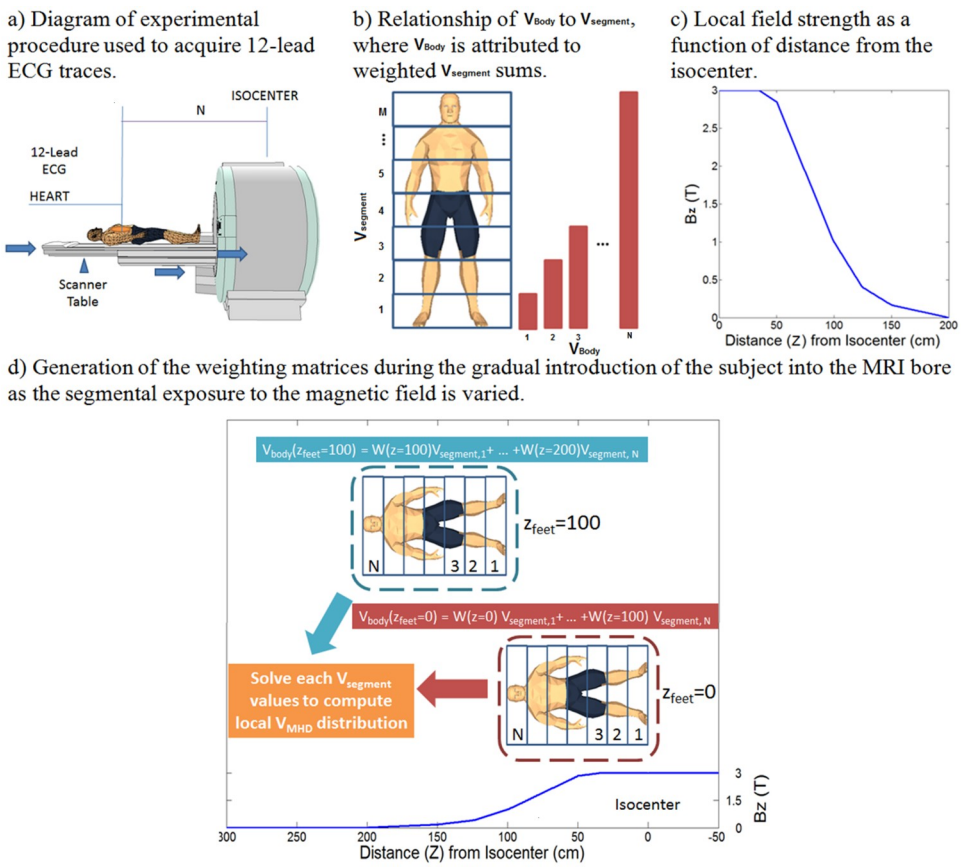

Fig 1. Recording of raw 12-lead ECG data for estimating regional contributions to the net V_{MHD} signal.

https://doi.org/10.1371/journal.pone.0213235.g001

The VCG frame of reference provided a direct visualization of the cardiac electrical signal vectors in 3-dimensional (3D) space, where the magnitude and direction of signals were referenced to a dipole center. The assumption of the dipole center point of reference has been shown to hold true despite the moving depolarization and repolarization wave-fronts that occur in the atria and ventricles during a normal cardiac cycle [26, 27]. V_{MHD} in the VCG representation can visualize the magnitude and direction of V_{MHD} at different locations in the myocardium at different points in the cardiac cycle in 3D (8–10 cm during ventricular contraction) and allows direct comparison with MRI data acquired in the MRI coordinate planes. The VCG frame of reference is used in clinical diagnosis of cardiac arrhythmias originating from varying sources within the heart (such as the ventricular wall), which superimpose signals onto the acquired VCG [28, 29]. In the environment of the MRI scanner, induced V_{MHD} signals are similarly superimposed onto the VCG, and are the basis for translating to this frame of reference for analysis. In addition, VCG vector format simplifies the subsequent signal processing from handling the 12 ECG traces to the 3 VCG traces.

V_{MHD} vector extraction was performed through the subtraction of VCGs obtained within the magnetic field at each displacement level ($\overrightarrow{ECG_{measured}(z)}$) from a constant reference, VCGs obtained with the subject completely outside of the MRI magnetic field acquired at the beginning of the procedure ($\overrightarrow{ECG_{reference}}$) (Eq 3). This serves to isolate the MHD signal contribution

from the contribution of the true time-integrated ECG [24].

$$\overrightarrow{V_{MHD}(z)} = \overrightarrow{ECG_{measured}(z)} - \overrightarrow{ECG_{reference}} \quad (3)$$

Time-integration of V_{MHD}, corresponding to V_{MHD} induced by systolic blood flow, over the cardiac S-wave to T-wave (S-T) segment was performed at each displacement level, providing a metric proportional to blood volume through systolic integration of flow. This serves as a beat-to-beat estimate for the body's contribution to the net recorded V_{MHD} (V_{body}) in the three component directions [24] (Eq 4), the magnitude of which is then taken at each level. We defined V_{body} as the time integral of the recorded V_{MHD} magnitude over the duration of the S-T segment at each displacement level.

$$V_{body} = \int_S^T |\overrightarrow{V_{MHD}(t)}|dt \quad (4)$$

The V_{body} metric can, therefore, be defined as the weighted summation of neighboring body segments ($V_{segment}$), totaling the net induced MHD voltage recorded at each displacement level or V_{body} (Fig 1b). Since V_{body} is influenced by the varying magnetic field strengths as a function of subject displacement from the isocenter (Fig 1c), normalization or weighting terms must be included for comparison of the contribution of each $V_{segment}$ (Eq 5). W(z) takes into account the spatial variation of the magnetic field ($B_0(z)$) at various distances from magnet isocenter (Fig 1d) [30, 31].

This summation of each weighted $V_{segment}$ term is performed over the entire height of the subject, forming a total of N discrete segments of equal length (t = 10 cm). Increases in N can result in higher spatial resolution for identifying the magnetohydrodynamic voltage distributions in the subject body.

$$W(z) = \frac{B_0(z)}{3T} \quad (5)$$

A linear decomposition was applied in order to resolve the weighted $V_{segment}$ from the V_{body} measured in incremental distances from isocenter (Eqs 6–7). Each $V_{segment}$ value was calculated at different body segments and scaled to be independent of applied magnetic field at each displacement level using $W(z)$. $V_{segment}$ values were calculated for each body segment of t cm, and repeatedly for N body regions (Fig 1d).

$$W(z)V_{segment} = V_{body} \quad (6)$$

$$\begin{bmatrix} W(z=0) & W(z=t) & W(z=2t) & \dots & W(z=Nt) \\ W(z=t) & W(z=2t) & W(z=3t) & \dots & W(z=(N+1)t) \\ W(z=2t) & W(z=3t) & W(z=4t) & \dots & W(z=(N+2)t) \\ \vdots & \vdots & \vdots & \ddots & \vdots \\ W(z=Nt) & W(z=(N+1)t) & W(z=(N+2)t) & \dots & W(z=2Nt) \end{bmatrix} \begin{bmatrix} V_{segment,(1)} \\ V_{segment,(2)} \\ V_{segment,\ (3)} \\ \vdots \\ V_{segment,N} \end{bmatrix} = \begin{bmatrix} V_{body}(z_{feet}=0) \\ V_{body}(z_{feet}=t) \\ V_{body}(z_{feet}=2t) \\ \vdots \\ V_{body}(z_{feet}=Nt) \end{bmatrix} \quad (7)$$

Statistical analysis

For each subject, an MRI angiogram was obtained prior to V_{MHD} processing for validation of obtained $V_{segment}$ traces; MR images were obtained using three-dimensional phase contrast balanced steady-state free precession (bSSFP) sequences without the injection of Gadolinium

contrast media, TR: 7, TE: 4, Flip Angle: 20 degrees, 8 mm slice thickness. Image reconstruction and processing was performed using the OsiriX DICOM Viewer (Pixmeo, Bernex, Switzerland). Maximum intensity projections (MIPs) were performed across the patient angiogram at 8 mm intervals, and a thoraco-abdominal trace was obtained from the MRI angiogram. The correlation between V_{MHD} and the MRA curves was quantified using Spearman's ranked correlation coefficient in both the abdominal and thoracic cavities.

Results

$V_{segment}$ was resolved in each subject (Fig 2b) and displayed as a function of the distance (displacement) from the subject's feet or height.

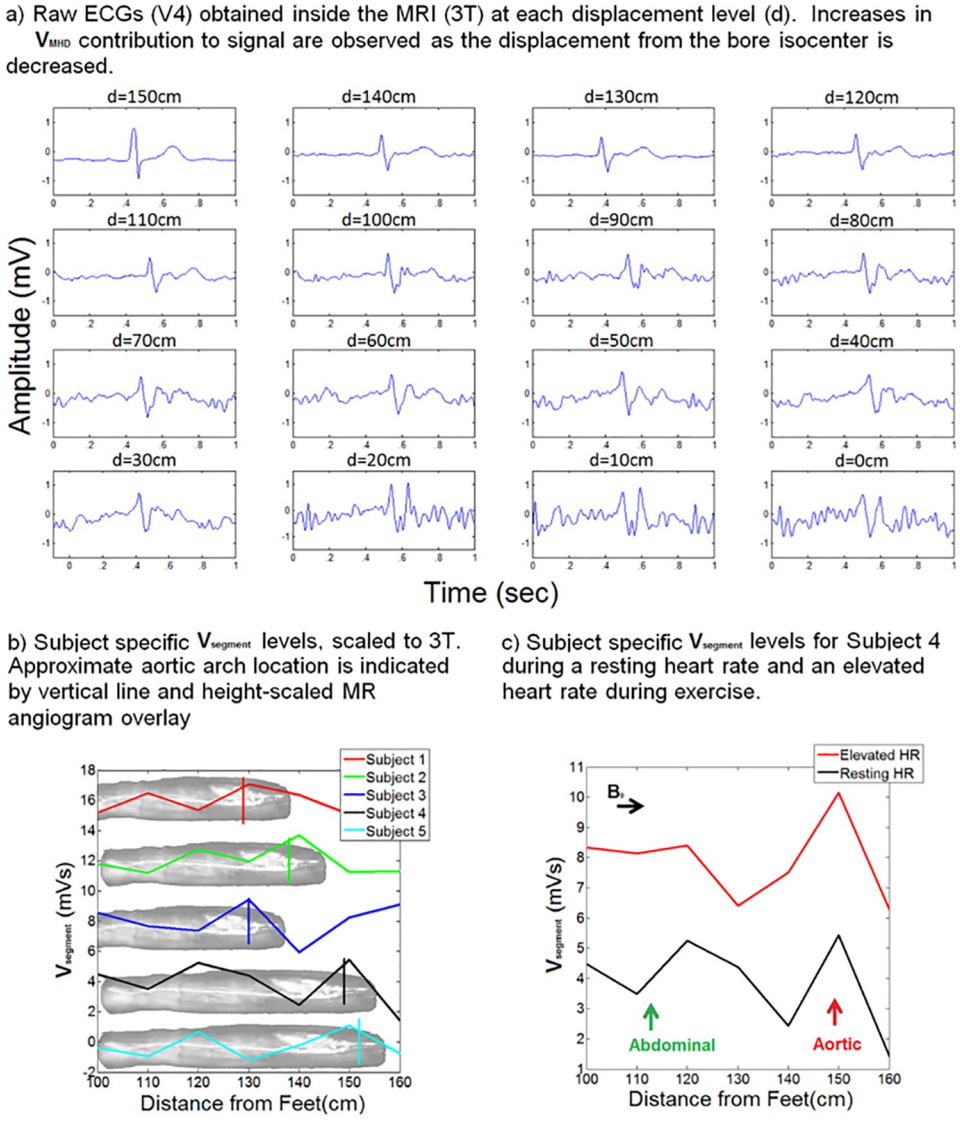

Fig 2. Derivation of subject-specific V_{MHD} based maps through the gradual introduction of the subject into the static magnetic field of the MRI.

https://doi.org/10.1371/journal.pone.0213235.g002

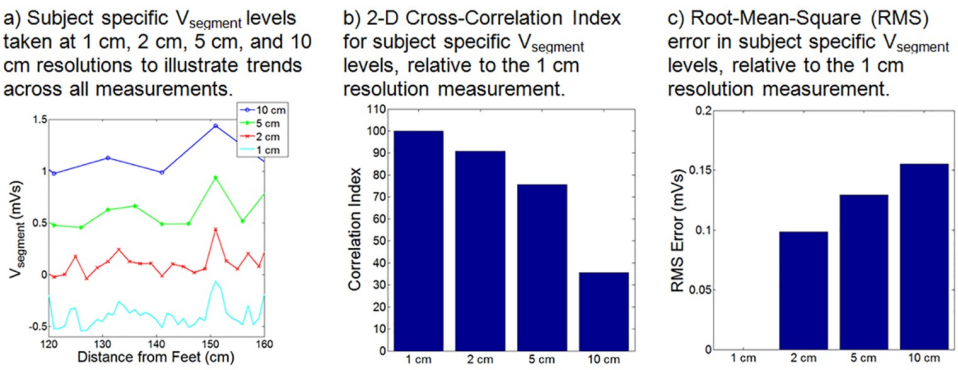

Fig 3. Subject specific $V_{segment}$ levels obtained for a single subject at 1 cm, 2 cm, 5 cm, and 10 cm resolutions.

https://doi.org/10.1371/journal.pone.0213235.g003

Extraction of MHD voltage distributions

$V_{segment}$ varied over the course of the different body segments, with the major blood vessels providing for greater changes in $V_{segment}$. Minimal $V_{segment}$ intensity was found in vasculature oriented mainly parallel to the magnetic field, where the direction of blood flow aligned with B_0 during the experimental procedure (Fig 2). This occurred for the abdominal aorta and the carotid artery in all subjects.

$V_{MHD,}$ attributed to rapidly flowing blood in the aortic arch during early systole, was shown to dominate $V_{segment}$ curves in all the subjects. A similar increase in V_{MHD} was observed due to blood volumes stored in the abdominal solid organs and fed by primary branches of the major vasculature (e.g. the abdominal aorta). The dataset obtained at the increased spatial resolution (1 cm) illustrated a similar trend as observed with the 10 cm resolution, as demonstrated by varying the spatial resolution of the acquired 1 cm high-resolution dataset to 2 cm, 5 cm, and 10 cm (Fig 3).

Fluctuations in $V_{segment}$ (Fig 3a), which were primarily observed as positive trace deflections, were associated with aortic-arch flow within the thoracic cavity, the main branches of the abdominal aorta, such as the renal, splenic, and hepatic arteries, as well as the bifurcation of the common iliac artery. The largest fluctuation was observed at the 150 cm mark, corresponding to the location where the aortic arch was approximately angled orthogonal to B_0.

A 50.6% increase in cardiac $V_{segment}$ was observed in subject 4 (Fig 2c) when the heart rate was elevated from a resting heart rate of 82 bpm to 114 bpm during exercise, corresponding to an increased level of blood flow during exercise.

Statistical analysis

MR angiograms were obtained for each subject and subsequent trace extraction was performed. MRA traces were compared to the extracted V_{MHD} traces, as determined in (1), to assess method validity and overlaid onto MRA magnitude images (Fig 4).

A significant correlation, 0.96 and 0.97 for abdominal and thoracic cavities, respectively, was found between the MRA and V_{MHD} derived traces, with a p-value of <0.001 using Spearman's ranked correlation coefficient, where a coefficient of 1 designates perfect correlation [32]. Comparison of V_{MHD}- and MRA-based traces yielded parallel positive signal deflections in the subject's superior thoracic cavity. These appeared at the level of the aortic arch, a known primary contributor to the net MHD voltage. Abdominal correlation is attributed to the large blood volume reserves contained in the abdominal solid organs, and the respective high

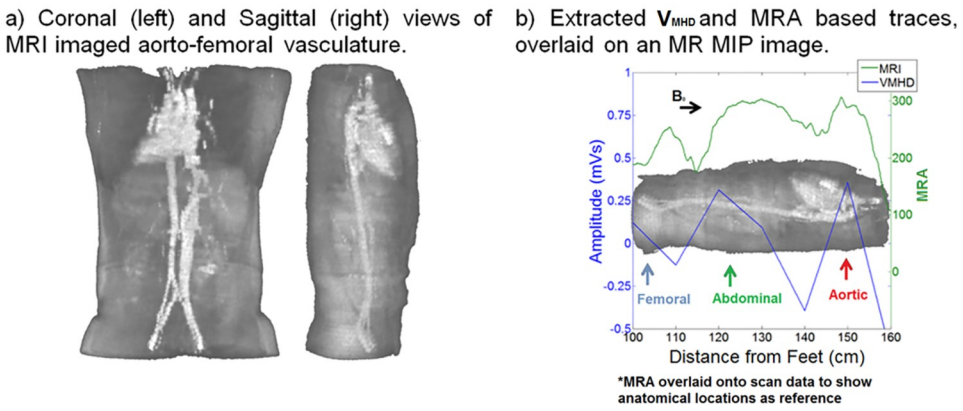

Fig 4. MRI validation of V_{MHD} based calculations using MR angiograms.

https://doi.org/10.1371/journal.pone.0213235.g004

blood-flow arterial branches out of the abdominal aorta. Renal, splenic, and hepatic branches of the abdominal aorta maintain large angles (~90 degrees) between the vasculature and the magnetic field direction, causing large increases in V_{MHD}, which match that seen in the MRA projections. The MHD voltage was therefore demonstrated to reflect the net effect of blood flow occurring within individual body regions, as recorded through surface ECGs, in a similar manner to that obtained through traditional MRA procedures.

Discussion

Subject specific $V_{segment}$ levels were extracted and shown to correlate with subject anthropometry. A high-resolution dataset was acquired (1 cm) and shown to correlate well with the standard 10 cm resolution measurements.

MRA-derived measurements were shown to agree well with V_{MHD}-based experimental data, excluding specific regions where the V_{MHD}-derived maps displayed lower blood flow, because the direction of blood flow in these regions was mainly parallel to the magnetic field.

The development of a rapid non-invasive measurement of patient blood-volume levels would allow physicians to more accurately detect changes in flow and blood volume across a wider population, including in patients with peripheral arterial disease or congestive heart failure. It is expected that the V_{MHD} maps would detect restricted flow cases.

As is true for any MRI procedure, patients with medical implants not labeled as MR conditional in the 3T field, would need to be excluded from this procedure. Additional patient safety concerns related to RF fields and static/gradient magnetic fields were previously studied and found to be limited to induced nausea during gross patient movements, which is considered as non-significant risk to patients at 3T [30, 31]. Moreover, in order for the proposed method to be accepted for use with patients with pathologies, such as those caused by cardiovascular diseases, it is important to understand the effects of magnetic fields on abnormal vasculature. For example, blood flow through stenosed arteries [33], irregular multi-stenosed arteries [34], and aneurysmal geometry [35] has been found to react to magnetic fields differently than blood flow through healthy vasculature, sometimes with complex responses.

Further studies to increase method accuracy and reduce the required acquisition time must be performed to integrate this technology into existing MR scanner platforms or to develop a standalone device for measuring blood volumes.

Limitations

This study is a feasibility study to explore the use of the MHD effect as a novel vascular metric. The limited population size in this study necessitates that the method be further validated in a larger population, including in patients diagnosed with cardiovascular diseases. The present work presents a proof of concept study for examining regional body contributions to the net recorded V_{MHD}.

The V_{MHD} maps may, however, also be influenced by other sources, such as large chest dimensions and increased layers of subcutaneous fat. Further studies must be performed to fully understand the role of variations in tissue electrical conductivity on the proposed methodology. Furthermore, the VCG frame of reference normally models the recorded V_{MHD} as originating in a single dipole source within the heart, whereas this study seeks to find contributions to the net V_{MHD} from several sources located far from the heart. In the case of V_{MHD} sources located near the SA node, which have comparable displacements of the detecting electrodes from the cardiac dipole source, such as the MHD voltage originating from the aortic arch, we have shown that this assumption is valid. Larger source displacements from the heart, such as those studied here, may require modifying the Dower Transform, and generating subject-specific coefficients. Subject-specific coefficients have been shown to provide increased accuracy relative to the generic coefficients [36]. We limited this study to the thoraco-abdominal cavity in order to reduce this variability. However, the merits of generating subject-specific coefficients should be further explored, since they may increase the accuracy of the blood-volume maps.

The presented method demonstrated the contributions of vasculature in the human body to the net MHD voltage, but did not provide a quantitative transfer-function between the resolved $V_{segments}$ and the true blood volume distributions. To completely develop this transfer function, a quantitative analysis is required to understand the relationship between the MHD voltages, the size and velocity of the vessels of interest, and the attenuation of electrical signal as they traverse through different tissue layers along its path from the MHD source to the surface-electrode detectors.

In addition, the current method is limited to V_{MHD} contributions from vasculature lying primarily perpendicular to the MRI's magnetic field direction. This is because when the blood flow is perpendicular to the magnetic field, the magnetic force on the blood is maximum. In contrast, when the blood flow is parallel to the magnetic field, there is no magnetic force on the blood, so the movement of the blood is not affected. Hence, V_{MHD} contributions from vasculature lying primarily parallel to the MRI's magnetic field direction are minimal. Therefore, the proposed method of using MHD for flow estimation is most sensitive to blood flow perpendicular to the magnetic field. In order to add contributions from vasculature that lie in other orientations, magnetic fields oriented in other directions could be added, which might be possible to perform by adding bucking coils outside the MRI bore.

Although the main field of MRI scanner is in the z direction, there are secondary magnetic fields in the x and y direction near the gantry of the MRI scanner, which can produce small undesirable MHD voltages and therefore affect the measurement accuracy. However, the undesirable MHD voltages are far away from the measurement electrodes, so the sensor will not pick up very much noise. In future studies we will explore a way to consider the x and y magnetic field in our computation for blood flow measurements.

The current method is based on Dower transform to convert ECG into VCG domain. The Dower transform is a well-known method for ECG conversion, but it makes assumption about the size, shape, electrical properties, and signal source of the parcel, which affects the accuracy

of the calculation. Future work will include multi-electrode measurements across the whole torso in order to produce more accurate MHD measurements.

Another limitation is that patients tend to have bad ECG measurements while exercising.

Measurements during heavy exercise tend to have severe noise interference and baseline rendering which can affect measurement accuracy.

Future Work

Further work to advance the utility of the study includes the development of a standalone device that is based on a portable magnetic field source and miniaturized ECG hardware, allowing for metric quantification in the absence of the MRI magnetic field. The methods presented will also be further validated in a larger subject population that contains both healthy subjects and patients with vascular diseases, such as peripheral arterial disease or congestive heart failure. Future work must be performed to map higher resolution V_{MHD}-derived features to MRI scan data, and to relate the MHD spatial decomposition to flow distributions in the body.

Conclusions

In this study, V_{MHD} signals were shown to correlate well with regional blood volumes, illustrating trends comparable to those from standard imaging methodologies. Although the scope of this study was limited, the preliminary results supported the proof of concept. Therefore, future studies are warranted to rigorously investigate the proposed method. Moreover, future studies should consider the integration of this method into a portable device to improve clinical workflows.

Author Contributions

Methodology: Jonathan R. Murrow.

Resources: John N. Oshinski.

Software: T. Stan Gregory.

Supervision: Zion Tsz Ho Tse.

References

1. Di Carli M, Czernin J, Hoh CK, Gerbaudo VH, Brunken RC, Huang S-C, et al. Relation among stenosis severity, myocardial blood flow, and flow reserve in patients with coronary artery disease. Circulation. 1995; 91(7):1944–51. PMID: 7895351
2. Association AH. Heart and stroke facts: The Association; 1993.
3. Heitzer T, Schlinzig T, Krohn K, Meinertz T, Münzel T. Endothelial dysfunction, oxidative stress, and risk of cardiovascular events in patients with coronary artery disease. Circulation. 2001; 104(22):2673–8. PMID: 11723017
4. Ku DN. Blood flow in arteries. Annual Review of Fluid Mechanics. 1997; 29(1):399–434.
5. Sowers JR, Epstein M, Frohlich ED. Diabetes, hypertension, and cardiovascular disease an update. Hypertension. 2001; 37(4):1053–9. PMID: 11304502
6. Weissler AM, Peeler RG, Roehll Jr WH. Relationships between left ventricular ejection time, stroke volume, and heart rate in normal individuals and patients with cardiovascular disease. American heart journal. 1961; 62(3):367–78.
7. Rendell MS, Milliken BK, Finnegan MF, Finney DA, Healy JC. The skin blood flow response in wound healing. Microvascular research. 1997; 53(3):222–34. https://doi.org/10.1006/mvre.1997.2008 PMID: 9211400
8. Wu KJ, Gregory TS, Reeder C, Leitmann B, Huffines A, Donovan S, et al. Smartphone-Enabled Device for the Monitoring of Blood Volume Variations using Magnetohydrodynamic Voltages. Circulation. 2015.

9. Kolin A. Electromagnetic Blood Flow Meters. Implantable flow transducers facilitate circulatory studies in conscious and free-moving animals. 1959; 130(3382):1088–97. https://doi.org/10.1126/science.130.3382.1088 PMID: 17736056
10. Krug JW, Rose G. Magnetohydrodynamic distortions of the ECG in different MR scanner configurations. Computing in Cardiology. 2011:769–72.
11. Gupta A, Weeks AR, Richie SM. Simulation of elevated T-waves of an ECG inside a static magnetic field (MRI). IEEE transactions on bio-medical engineering. 2008; 55(7):1890–6. https://doi.org/10.1109/TBME.2008.919868 PMID: 18595808.
12. Nijm G, Swiryn S, Larson A, Sahakian A. Extraction of the magnetohydrodynamic blood flow potential from the surface electrocardiogram in magnetic resonance imaging. Med Biol Eng Comput. 2008; 46:729–33. https://doi.org/10.1007/s11517-008-0307-1 PMID: 18239947
13. Nijm G, Swiryn S, Larson A, Sahakian A, editors. A 3D model of magnetohydrodynamic voltages: comparison with voltages observed on the surface ECG during cardiac MRI. Computers in Cardiology, 2007; 2007: IEEE.
14. Frauenrath T, Fuchs K, Dieringer MA, Ozerdem C, Patel N, Renz W, et al. Detailing the use of magnetohydrodynamic effects for synchronization of MRI with the cardiac cycle: a feasibility study. Journal of magnetic resonance imaging: JMRI. 2012; 36(2):364–72. https://doi.org/10.1002/jmri.23634 PMID: 22411274.
15. Togawa T, Okai O, Oshima M. Observation of blood flow EMF in externally applied strong magnetic field by surface electrodes. Medical and Biological Engineering and Computing. 1967; 5(2):169–70.
16. Gregory T, Schmidt E, Zhang S, Tse Z. 3DQRS: A method to obtain reliable QRS complex detection within high field MRIs using 12-lead ECG traces. Magnetic Resonance in Medicine. 2014; 71(4):1374–80. https://doi.org/10.1002/mrm.25078 PMID: 24453116
17. Gregory TS, Schmidt EJ, Zhang SH, Kwong RY, Stevenson WG, Murrow JR, et al. Left-Ventricular Mechanical Activation and Aortic-Arch Orientation Recovered from Magneto-Hydrodynamic Voltages Observed in 12-Lead ECGs Obtained Inside MRIs: A Feasibility Study. Annals of Biomedical Engineering. 2014; 42(12):2480–9. https://doi.org/10.1007/s10439-014-1109-2 PMID: 25224074
18. Gregory TS, Oshinski J, Schmidt EJ, Kwong RY, Stevenson WG, Tse ZTH. Continuous Rapid Quantification of Stroke Volume Using Magnetohydrodynamic Voltages in 3T Magnetic Resonance Imaging. Circulation: Cardiovascular Imaging. 2015; 8(12):e003282. https://doi.org/10.1161/CIRCIMAGING.115.003282 PMID: 26628581
19. Buchenberg WB, Mader W, Hoppe G, Lorenz R, Menza M, Büchert M, et al. In vitro study to simulate the intracardiac magnetohydrodynamic effect. Magnetic Resonance in Medicine. 2015; 74(3):850–7. https://doi.org/10.1002/mrm.25456 PMID: 25224650
20. Oster J, Llinares R, Payne S, Tse ZTH, Schmidt EJ, Clifford GD. Comparison of three artificial models of the magnetohydrodynamic effect on the electrocardiogram. Computer methods in biomechanics and biomedical engineering. 2015; 18(13):1400–17. https://doi.org/10.1080/10255842.2014.909090 PMID: 24761753
21. Abi Abdallah D, Drochon A, Robin V, Fokapu O. Effects of static magnetic field exposure on blood flow. The European Physical Journal Applied Physics. 2009; 45(01):11301.
22. Abi-Abdallah D, Robin V, Drochon A, Fokapu O. Alterations in human ECG due to the MagnetoHydro-Dynamic effect: a method for accurate R peak detection in the presence of high MHD artifacts. Conference proceedings: Annual International Conference of the IEEE Engineering in Medicine and Biology Society IEEE Engineering in Medicine and Biology Society Conference. 2007:1842–5. https://doi.org/10.1109/IEMBS.2007.4352673 PMID: 18002339.
23. Birkholz T, Schmid M, Nimsky C, Schuttler J, Schmitz B. ECG artifacts during intraoperative high-field MRI scanning. Journal of neurosurgical anesthesiology. 2004; 16(4):271–6. PMID: 15557829.
24. Tse Z, Dumoulin CL, Clifford GD, Schweitzer J, Qin L, Oster J, et al. A 1.5T MRI-conditional 12-lead electrocardiogram for MRI and intra-MR intervention. Magn Reson Med. 2013; 71(3):1336–47.
25. Dower GE. The ECGD—a Derivation of the ECG from VCG Leads. J Electrocardiol. 1984; 17(2):189–91. PMID: 6736842
26. Arthur RM, Geselowitz DB, Briller SA, Trost RF. The path of the electrical center of the human heart determined from surface electrocardiograms. J Electrocardiol. 1971; 4(1):29–33. PMID: 5559848
27. Savard P, Roberge FA, Perry J-B, Nadeau RA. Representation of cardiac electrical activity by a moving dipole for normal and ectopic beats in the intact dog. Circ Res. 1980; 46:415–25. PMID: 7357696
28. Benchimol A, Pedraza A. The timed Frank vectorcardiogram in the diagnosis of cardiac arrhythmias. J Electrocardiol. 1969; 2(4):363–72. PMID: 4191909
29. Frank E. An accurate, clinically practical system for spatial vectorcardiography. Circulation. 1956; 13(5):737–49. PMID: 13356432

30. Kännälä S, Toivo T, Alanko T, Jokela K. Occupational exposure measurements of static and pulsed gradient magnetic fields in the vicinity of MRI scanners. Physics in medicine and biology. 2009; 54 (7):2243–57. https://doi.org/10.1088/0031-9155/54/7/026 PMID: 19293469

31. Laakso I, Kännälä S, Jokela K. Computational dosimetry of induced electric fields during realistic movements in the vicinity of a 3T MRI scanner. Physics in medicine and biology. 2013; 58(8):2625–40. https://doi.org/10.1088/0031-9155/58/8/2625 PMID: 23552657

32. Press WH, Teukolsky SA, Vetterling WT, Flannery BP. Numerical recipes in C: Cambridge University Press; 1996.

33. Rusli N, Kueh ABH, Kenjeres S. Magnetic field effects on 3D blood flow patterns of straight and stenotic arteries. Advanced Science Letters. 2013; 19(9):2690–3.

34. Mustapha N, Amin N, Chakravarty S, Mandal PK. Unsteady magnetohydrodynamic blood flow through irregular multistenosed arteries. Computers in Biology and Medicine. 2009; 39(10):896–906. PMID: 19665698

35. Raptis A, Xenos M, Tzirtzilakis E, Matsagkas M. Finite element analysis of magnetohydrodynamic effects on blood flow in an aneurysmal geometry. Physics of Fluids. 2014; 26(10).

36. Huiskamp G, Van Oosterom A. Tailored versus realistic geometry in the inverse problem of electrocardiography. IEEE transactions on bio-medical engineering. 1989; 36(8):827–35. https://doi.org/10.1109/10.30808 PMID: 2759641